

Deciphering the Role of Anions and Secondary Coordination Sphere in Tuning Anisotropy in Dy(III) Air-Stable D_{5h} SIMs**

Sandeep K. Gupta,^[a] Sourav Dey,^[a] Thayalan Rajeshkumar,^[a] Gopalan Rajaraman,^{*[a]} and Ramaswamy Murugavel^{*[a]}

Dedicated to Professor Arunachalam Ramanan on the occasion of his 65th birthday

Abstract: Precise control of the crystal field and symmetry around the paramagnetic spin centre has recently facilitated the engineering of high-temperature single-ion magnets (SIMs), the smallest possible units for future spin-based devices. In the present work, we report a series of air-stable seven coordinate Dy(III) SIMs $\{[L_2Dy(H_2O)_5][X]_3 \cdot L_2 \cdot n(H_2O), n = 0, X = Cl (1), n = 1, X = Br (2), I (3)\}$ possessing *pseudo- D_{5h}* symmetry or pentagonal bipyramidal coordination geometry with high anisotropy energy barrier (U_{eff}) and blocking temperature (T_B). While the strong axial coordination from the sterically encumbered phosphonamide, ^tBuPO(NH^tPr)₂ (L), increases the overall anisotropy of the system, the presence of high symmetry significantly quenches quantum tunnelling of magnetization, which is the prominent deactivating factor

encountered in SIMs. The energy barrier (U_{eff}) and the blocking temperature (T_B) decrease in the order $3 > 2 > 1$ with the change of anions from larger iodide to smaller strongly hydrogen-bonded chloride in the secondary coordination sphere, albeit the local coordination geometry and the symmetry around the Dy(III) display only slight deviations. *Ab initio* CASSCF/RASSI-SO/SINGLE_ANISO calculations provide deeper insights into the dynamics of magnetic relaxation in addition to the role of the secondary coordination sphere in modulating the anisotropy of the D_{5h} systems, using diverse models. Thus, in addition to the importance of the crystal field and the symmetry to obtain high-temperature SIMs, this study also probes the significance of the secondary coordination sphere that can be tailored to accomplish novel SIMs.

Introduction

Single-molecule magnets (SMMs) are superparamagnetic molecules that behave as molecular-level classical magnets at low temperatures.^[1] This scripts them as potential candidates for the fabrication of next-generation high-density data storage devices.^[2] Besides, they are also recognized as prospective candidates for application in future molecular spintronics and quantum computing due to the observance of phenomena such as quantum tunneling of magnetization (QTM) and quantum phase interference.^[3] However, these properties are witnessed only at very low temperatures in most SMMs, thus rendering them unfit for technological applications. While the first slow relaxation of magnetization in a molecular complex was observed in an 'Mn₁₂' cluster,^[4] the report on high energy

barrier (U_{eff}) in the double-decker complexes, $[Pc_2Tb]^- [TBA]^+$, by Ishikawa et al. in 2003 shifted the attention to lanthanide ions for designing SMMs with high U_{eff} .^[5]

In the last decade, several groups have made remarkable efforts to decrypt the factors that can aid the synthesis of SMMs with higher blocking energy barriers (U_{eff}) and blocking temperatures (T_B). Particularly lanthanide ions having electronic configurations greater than $4f^7$ such as Dy(III), Er(III), and Tb(III) are more attractive due to large spin-orbit (SO) coupling and larger magnetic moments (as the f-orbitals are deeply buried and shielded, they do not significantly interact with the crystal field (CF)).^[1d,6] However, the presence of significant QTM in the case of 4f complexes between the ground state doublets significantly inhibits the slow relaxation of magnetization. QTM has been quenched by either incorporating a radical that induces a strong exchange coupling or a 3d metal ion in the complex.^[7] QTM has also been quenched either by maintaining a strong axiality and/or a higher-order symmetry.^[1d,6c,f,8] In 2011, Rinehart and Long put forward an idea based on the electrostatic model that proposed that a specific CF could be designed to enhance the anisotropic charge distribution of 4f ions.^[6a] While strong axial coordination makes oblate ions such as Dy(III), Tb(III), etc., more anisotropic, the reverse is true for ions with prolate electronic charge distribution. Thus, a better understanding of the elements that play a decisive role in realizing the slow relaxation dynamics such as the effect of

[a] Dr. S. K. Gupta, S. Dey, Dr. T. Rajeshkumar, Prof. G. Rajaraman, Prof. R. Murugavel
Department of Chemistry
Indian Institute of Technology Bombay
Powai, Mumbai, 400 076 (India)
E-mail: rajaraman@chem.iitb.ac.in
rmv@chem.iitb.ac.in

[**] A previous version of this manuscript has been deposited on a preprint server (<https://doi.org/10.33774/chemrxiv-2021-h3qk7>).

Supporting information for this article is available on the WWW under <https://doi.org/10.1002/chem.202103585>

crystal field (CF) and the symmetry in addition to the synthetic efforts, has resulted in SMMs with U_{eff} and T_{B} values as high as 1541 cm^{-1} and 80 K, respectively in a dysprosocenium complex.^[8d] While maintaining a strict axial symmetry seems to readily impart a very high anisotropic barrier in Ln(III) SIMs as recently reported in some interesting D_{4h} , D_{5h} , D_{6h} symmetric systems, the nature of axial ligand and geometry around the central Ln(III) ion seems to be very important to obtain higher blocking temperatures.^[6d,f,8a,9] While D_{4h} and D_{6h} systems appear to impart very high U_{eff} , they suffer from significant QTM at zero-field as observed in the magnetic hysteresis loop measurements.^[9d-f] Thus, the high U_{eff} does not always translate in high T_{B} . Moreover, apart from possessing high U_{eff} and T_{B} , these molecules also need to retain additional properties such as stability, solution processability and sublimability for fabrication. Therefore, it becomes necessary to outline design strategies to synthesize air-stable SIMs/SMMs.

In the present work, we report a series of air-stable pseudo- D_{5h} symmetric Dy(III) SIMs, $\{[\text{L}_2\text{Dy}(\text{H}_2\text{O})_5][\text{X}]_3 \cdot \text{L}_2 \cdot n(\text{H}_2\text{O}), n = 0, \text{X} = \text{Cl} (1), n = 1, \text{X} = \text{Br} (2), \text{I} (3)\}$, that exhibit high anisotropy energy barrier (U_{eff}) and blocking temperature (T_{B}). These SIMs have been rationally designed from a sterically encumbered phosphonamide ${}^t\text{BuPO}(\text{NH}^i\text{Pr})_2$. This study particularly unravels the role of halide ions in the secondary coordination sphere in fine-tuning the magnetic properties. The effect of coordinated halide anions on the SIM properties of 3d and 4f ions has been recently reported.^[10] The magnetic properties of complex 3 have been reported by our group in a previous communication.^[6f] These SIMs possess some of the highest U_{eff} and T_{B} values for any air-stable 3d or 4f systems. Additional *ab initio* calculations were performed to disclose the role of the phosphonamide ligand, secondary coordination sphere, and the higher-order symmetry in the realization of unique properties exhibited by these complexes.

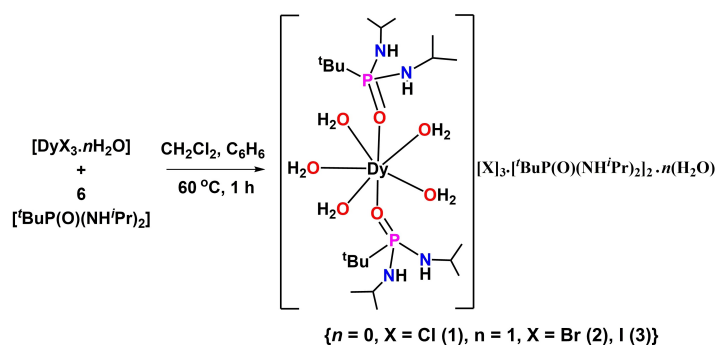
Results and Discussion

Synthetic aspects and molecular structures

The sterically bulky phosphonic diamide, ${}^t\text{BuPO}(\text{NH}^i\text{Pr})_2$ (L), was derived from the reaction of tert-butylphosphonic dichlor-

ide, ${}^t\text{BuPOCl}_2$, and excess isopropyl amine employing a literature procedure.^[11] The pentagonal-bipyramidal dysprosium complexes, $\{[\text{L}_2\text{Dy}(\text{H}_2\text{O})_5][\text{X}]_3 \cdot \text{L}_2 \cdot n(\text{H}_2\text{O}), n = 0, \text{X} = \text{Cl} (1), n = 1, \text{X} = \text{Br} (2), \text{I} (3)\}$, were synthesized from the direct reaction of the corresponding lanthanide halide hydrates with six equivalents of the ligand (Scheme 1). The compounds were obtained as crystals at ambient aerobic conditions via the slow evaporation of the reaction mixture. The structurally analogous Y(III) complexes were synthesized using similar synthetic protocol $\{[\text{L}_2\text{Y}(\text{H}_2\text{O})_5][\text{Cl}]_3 \cdot \text{L}_2 \cdot \text{CH}_2\text{Cl}_2 (4), [\text{L}_2\text{Y}(\text{H}_2\text{O})_5][\text{X}]_3 \cdot \text{L}_2 \cdot \text{H}_2\text{O}, \text{X} = \text{Br} (5), \text{I} (6)\}$. Crystals obtained from the mother liquor were separated and characterized by both analytical and spectroscopic techniques. All the complexes display a broad IR band around 3300 cm^{-1} corresponding to the N–H stretching vibrations (Figure S1). Two strong characteristic P=O bands were observed at around 1100 cm^{-1} for all the complexes due to the presence of two types of P=O bonds, one in the lattice and the other coordinated to the metal ion.

Single crystal X-ray diffraction analyses reveal that all the three complexes have a similar core structure around the central Dy(III) ion, whilst some differences are found in the arrangement of the anions and the neutral lattice ligands in the secondary coordination sphere. Complex 1, $[\text{L}_2\text{Dy}(\text{H}_2\text{O})_5][\text{Cl}]_3 \cdot \text{L}_2$, crystallizes in the orthorhombic space group $Pbca$. The asymmetric part of the unit cell contains one seven coordinate dysprosium ion coordinated to two phosphonic amide ligands and five water molecules (Figure 1). In addition, there are two phosphonic amide ligands present in the lattice along with three chloride anions, which balance the overall charge. The coordination sites in the equatorial plane of the dysprosium ion are occupied by the water molecules and the axial sites are coordinated by the phosphoryl oxygen atom of the amide ligand. Analysis of the $\{\text{DyO}_7\}$ core ion using SHAPE 2.1^[12] shows the least deviation (0.492) from the D_{5h} symmetry suggesting that Dy(III) ion occupies a distorted pentagonal bipyramidal coordination environment (Figure 2 and Table S2). The axial Dy–O(P) distances (2.203(1) and 2.213(1) Å) are shorter than the equatorial Dy–O(aqua) distances (2.335(2)–2.407(2) Å). This, in addition to the near-linear *trans* O(P)–Dy–O(P) angle (172.19(6)°), renders a virtual *quasi-two* coordinate coordination environment to the Dy(III) ion, a highly sought after geometry in the case of 4f-SMMs.^[13] The two Dy–O–P angles are



Scheme 1. Synthesis of the seven coordinate Dy(III) complexes of the phosphonic diamide ligand.

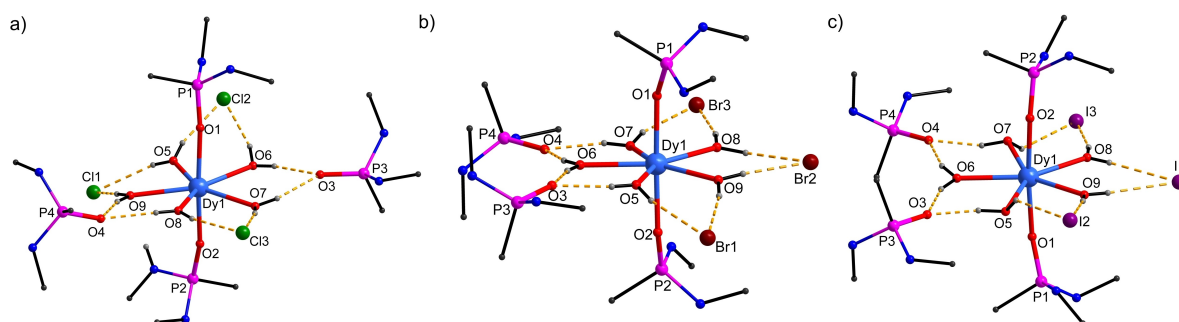


Figure 1. Molecular structures of the *pseudo-D*_{5h} dysprosium(III) complexes 1–3 (a–c). Lattice water molecule, methyl groups, and H-atoms attached to carbon and nitrogen centres have been omitted for clarity. The H-atoms of the water molecules are hydrogen bonded to the halide anions and lattice phosphonic diamide ligands forming a star-like architecture. Dashed yellow bonds indicate H-bonding.

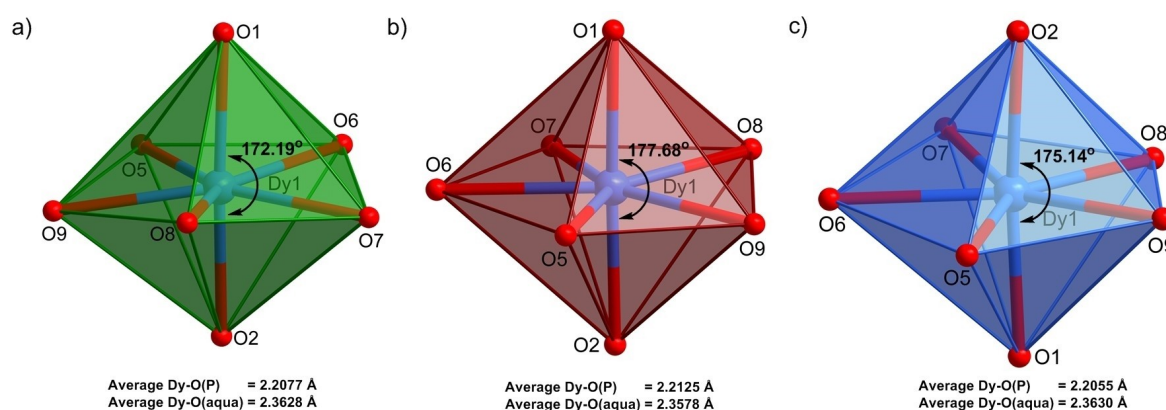


Figure 2. Comparative polyhedral view of the pentagonal bipyramidal coordination environment of Dy(III) ion in 1–3 (a–c) with ligating oxygen atoms.

169.53(1)° and 166.89(1)°. The hydrogen atoms of the water molecules coordinated to the Dy(III) ion are hydrogen-bonded to three chloride anions and two neutral phosphonic diamide ligands giving a star-like H-bonded architecture (Figure 1). The closest Dy(III)–Dy(III) distance in the lattice of 9.815 Å is largely aided by the presence of two uncoordinated phosphonic diamide ligands and the three lattice chloride ions present per formula unit. The chloride ions are further involved in weak H-bonding with the amide protons giving rise to a two-dimensional network of mononuclear dysprosium complexes (Figure S2).

Complexes 2 and 3 crystallize in the triclinic space group $P\bar{1}$ and are isomorphous. While the primary coordination sphere around the Dy(III) ion in 2 and 3 have similar core structural features as in complex 1 (Figure 1, 2, and Table 1), they differ in the arrangement of the non-coordinated three lattice anions and two phosphonic amide ligands in the second coordination sphere. Besides, one molecule of water is present in the lattice. The *trans* O(P)–Dy–O(P) angle is more linear in 2 (177.68(8)°) and 3 (175.14(9)°) compared to 1. However, the major difference appears in the bent P–O–Dy angle, where the bent angle is more linear in the case of 1. This also leads to the decrease of the distance of phosphorous atom from the mean {DyO₅}

Table 1. Comparative bond lengths, bond angles and other structural parameters in 1–3.

Complex	1	2	3
Trans O–Dy–O angle [°]	172.19(6)	177.68(8)	175.14(9)
Dy–O(P) distance [Å]	2.2029(1), 2.2125(1)	2.218(2), 2.207(2)	2.208(2), 2.203(2)
Dy–O(aqua) distance [Å]	2.3353(2)–2.4071(2)	2.343(2)–2.374(2)	2.355(3)–2.375(3)
Average Dy–O(aqua) distance [Å]	2.363	2.358	2.363
P–O–Dy angle [°]	169.53(1), 166.89(1)	149.29(1), 156.35(1)	149.72(1), 155.17(2)
Equatorial O–Dy–O angles [°]	69.91(7)–73.63(7)	69.94(8)–73.47(8)	70.43(9)–73.52(1)
Sum of equatorial O–Dy–O angles [°]	361.15	360.3	360.31
Average equatorial O–Dy–O angles [°]	72.23	72.06	72.062
Nearest Dy–Dy distance in the lattice [Å]	9.82	10.46	10.82
Average Dy–X distance [Å]	4.556	4.803	5.038
Average nearest X–O(aqua) distance [Å]	3.073	3.23075	3.446

equatorial plane in **2** and **3** as compared to **1**. With increasing anion size, the average Dy(III)⋯X and X⋯O(aqua) distances increase (X = halide). This also results in a considerable increase of nearest Dy(III)⋯Dy(III) distance in the crystal lattices of **2** (10.459 Å) and **3** (10.819 Å). Further, the increase in the ionic size of the lattice anions leads to the weakening of X⋯H—O hydrogen bonds in **2** and **3** (see Supporting Information). Analysis of the {DyO₇} core with the standard symmetry using SHAPE 2.1^[12] suggests an almost ideal *D*_{5h} symmetry with a deviation of 0.18 and 0.223 for **2** and **3**, respectively (Table S2). The corresponding diamagnetic Y(III) complexes **4–6** also reveal similar core structural features. While complex **4** crystallizes in the monoclinic space group *P*2₁/*c*, complexes **5** and **6** crystallize in the triclinic space group *P* $\bar{1}$ as in the case of their dysprosium analogues.

Magnetic Studies

The static and dynamic magnetic susceptibility measurements of **1–3** have been carried out using an MPMS-XL SQUID magnetometer. The direct current (dc) susceptibility measurements carried out on a polycrystalline sample under an applied magnetic field of 1000 Oe shows $\chi_{\text{M}}T$ values of 14.09, 13.90, and 14.15 cm³ K mol⁻¹ at 300 K for **1–3**, respectively, which is close to the estimated value of 14.18 cm³ K mol⁻¹ for an isolated Dy(III) ion (ground state = ⁶H_{15/2}) (Figure S9). The $\chi_{\text{M}}T$ values of **1–3** remain almost constant with lowering of the temperature but fall sharply near 10 K indicating a large energy separation among the low-lying Kramers doublets (KDs), indicating magnetic blocking. The field (*H*) dependent magnetization (*M*) curve for **1–3** shows a sinusoidal behavior (Figure S10), a signature of large anisotropy, with a steep increase in magnetization at the lower field before reaching ~5.0 μ_{B} at 7.0 T as seen in several high-temperature SMMs.^[6f]

Alternating current (ac) susceptibility measurements were carried out to unravel the slow relaxation dynamics of **1–3** at zero applied dc field between 0.1 and 1500 Hz at an oscillating ac field of 3.5 Oe. Clear frequency and temperature-dependent maxima in the out-of-phase signals were observed up to 36~40 K for **1–3** indicative of a very high thermal energy barrier. Maxima in the out-of-phase component of the frequency-dependent ac susceptibility (χ_{M}'') signals were observed up to 36 K for **1** indicative of a very high thermal energy barrier (Figure 3). To extract the relaxation times, the ac susceptibilities were fitted with a generalized Debye model which shows a temperature-dependent regime at higher temperatures. A linear fit of the temperature-dependent relaxation times (τ) at high temperatures to the Arrhenius law yields $U_{\text{eff}}=582(13)$ K and $\tau_0=1.4(6)\times 10^{-11}$. However, complex **1** shows a linear behavior only until 30 K and deviates from linearity at lower temperatures indicating the presence of other competing relaxation processes. Thus the relaxation times extracted over the entire temperature range were treated considering the QTM, direct, Raman, and Orbach processes with the following expression:^[14]

$$\tau^{-1} = \tau_{\text{QTM}}^{-1} + AT + CT^n + \tau_0^{-1} \exp\left(-\frac{U_{\text{eff}}}{k_{\text{B}}T}\right) \quad (1)$$

The best fit to Equation (1) for **1** yields an anisotropy barrier U_{eff} of 609(4) K with $\tau_0=6.6(6)\times 10^{-12}$ s, relative to the Orbach process with further contribution from the Raman relaxation mechanism ($C=2.0(7.0)\times 10^{-4}$ s⁻¹ K⁻ⁿ, $n=3.6(1.1)$). This indicates that the QTM is effectively quenched due to the high symmetry around the Dy(III) ion and strong axial CF. The application of dc fields shows only a slight effect on the energy barrier (Figure S11). Complex **2** also displays similar relaxation dynamics like complex **1**, nevertheless, the maxima in the out-of-phase are shifted towards higher temperature (~39.0 K) while deviating from linearity below 30 K (Figure S15). The best fit to Equation (1) for **2** yields an anisotropy barrier U_{eff} of 640(20) K with $\tau_0=1.1(8)\times 10^{-11}$ s, relative to Orbach process with further contribution from the Raman relaxation pathway ($C=7.2(5)\times 10^{-7}$ s⁻¹ K⁻ⁿ, $n=4.7$) as observed in the case of complex **1**. As in the previous case, the application of dc fields has only negligible effects on the energy barrier (Figure S16). A detailed comparative magnetic study of complex **3** along with the isomorphous Er(III) complex has been reported already in a previous communication.^[6f] Thus, among the series, U_{eff} decreases in the order **3** > **2** > **1** with the change of anions from larger iodide to smaller chloride in the secondary coordination sphere. These results are interesting as we find that although the local coordination environment in **1–3** is the same, the replacement of halide anions in the secondary coordination sphere results in higher U_{eff} in the order **3** > **2** > **1**. This points out that the presence of higher negative charges in the equatorial position of oblate Ln(III) such as Dy(III) are detrimental to the effective U_{eff} .

To further ascertain the effect of halide ions on the SIM properties of these Dy(III) complexes, additional magnetic measurements were carried out. For example, zero-field cooled (ZFC)-field cooled (FC) variable temperature magnetization measurements were carried out to determine the blocking temperature (T_{B}) of **1–3** (Figure 4 a–d). Unlike ordered magnets where the effect arises from the long-range magnetic ordering, the magnetic blocking is completely molecular in origin in SMMs. At a certain temperature, the measurement timescale is inadequate for complete magnetic relaxation i.e., for the magnetization to flip over the energy barrier and reverse its spin direction. This results in the observance of hysteresis and blocking temperature (T_{B}) in SMMs. At T_{B} , the magnetic moments of the anisotropic molecules are no more in parallel orientation due to thermal excitations to higher excited states resulting in spin disorientation. This has been observed in few Ln(III)-based SIMs.^[8] T_{B} is defined as the maxima in the ZFC curve.^[1a] As can be seen from Figure 4, **3** possess the highest blocking temperature among the series. While T_{B} for **3** is 12.9 K (measured at a sweep rate of 2 K min⁻¹), **2** and **1** possess T_{B} of 11.6 K and 8.2 K, respectively. It is to be noted that the maxima in ZFC curves are highly dependent on the sweep rate (Figure 4d). T_{irr} for **1**, **2**, and **3** are 14.7 K, 13.2 K, and 9.2 K, respectively. To further compare the magnetic blocking in **1–3**,

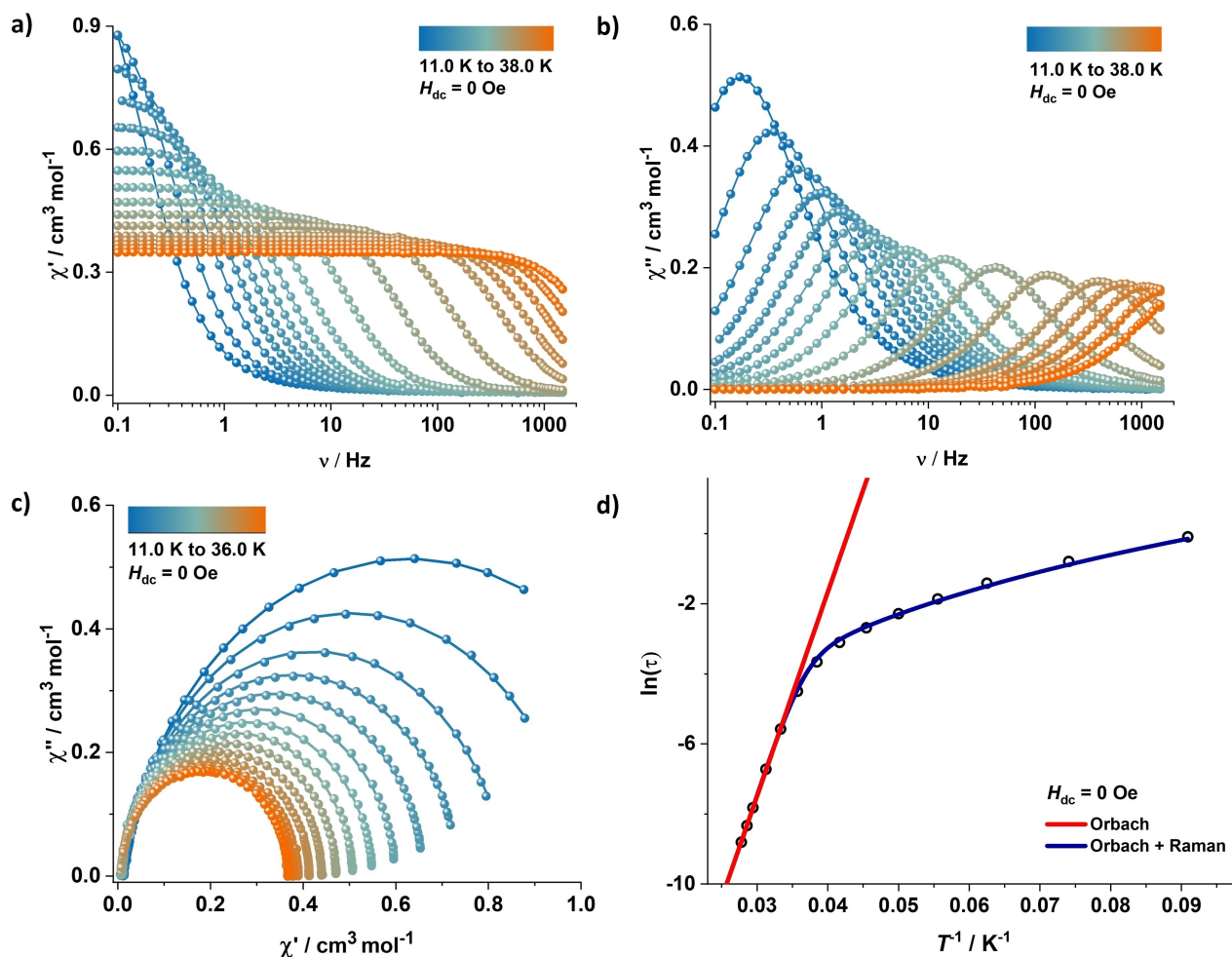


Figure 3. (a) In-phase (χ'_M) and (b) out-of-phase (χ''_M) components of frequency dependent ac susceptibility measured in an oscillating ac field of 3.5 Oe and zero applied dc field for **1**. (c) Cole-Cole plot for **1**. Solid lines are the best fit to the Debye model. (d) Plot of the relaxation time τ (logarithmic scale) versus T^{-1} obtained for **1**; the red line corresponds to the fitting of the Orbach relaxation process and the solid blue line represents the best fitting to the Orbach and Raman relaxation pathways.

magnetic hysteresis measurements were carried out. Similar to the effect of sweep rate for ZFC-FC experiments, the opening of the hysteresis loop and coercivity are highly dependent on the magnetic field sweep rate (Figure 4h). Among the series, **1** possesses significant tunneling around zero-field as against **2** and **3**. Larger consequences are especially seen in magnetic coercivity. The coercivity in the case of **1** is the least. **1**, **2**, and **3** display the opening of the hysteresis loop until 16.0 K, 14.0 K, 9.0 K, respectively (at a field sweep rate of 20 Oe s⁻¹). A comparative summary of the magnetic data is presented in Figure 5. Compared to **3**, some elegant examples of air-stable D_{4h} and D_{6h} systems reported recently with U_{eff} higher than 1800 K suffer from more substantial QTM at zero-field, significantly diminishing the observed coercivity, and the U_{eff} is not fully translated into T_B .^[9d-f] The combined properties (U_{eff} , T_B along with high coercivity) along with air and moisture stability place these SIMs amongst the best performing SIMs that are stable to air and moisture.

To further understand the relaxation dynamics, we prepared a 10% diluted sample (**2@Y** and **3@Y**) with the isomorphous Y(III) analogues. However, **2@Y** and **3@Y** display similar magnetic properties as **2** and **3**, thanks to the bulky phosphonic diamide ligands that keep the magnetic centers far apart in the crystal lattice. No significant improvement in blocking temperature and hysteresis was observed for **2@Y** and **3@Y** (Figures S23–S28). Hence the effect of dipolar exchange coupling interactions between the Dy(III) ions is also expected to be very weak. This further indicates that the observed magnetic properties observed in the present systems are completely molecular in nature and do not arise from any long-range ordering.

Electronic structure calculations

To comprehend the effect of counter anion on the magnetic properties, we have performed *ab initio* CASSCF/RASSI-SO/SINGLE_ANISO calculations on complexes **1**, **2**, and **3** using

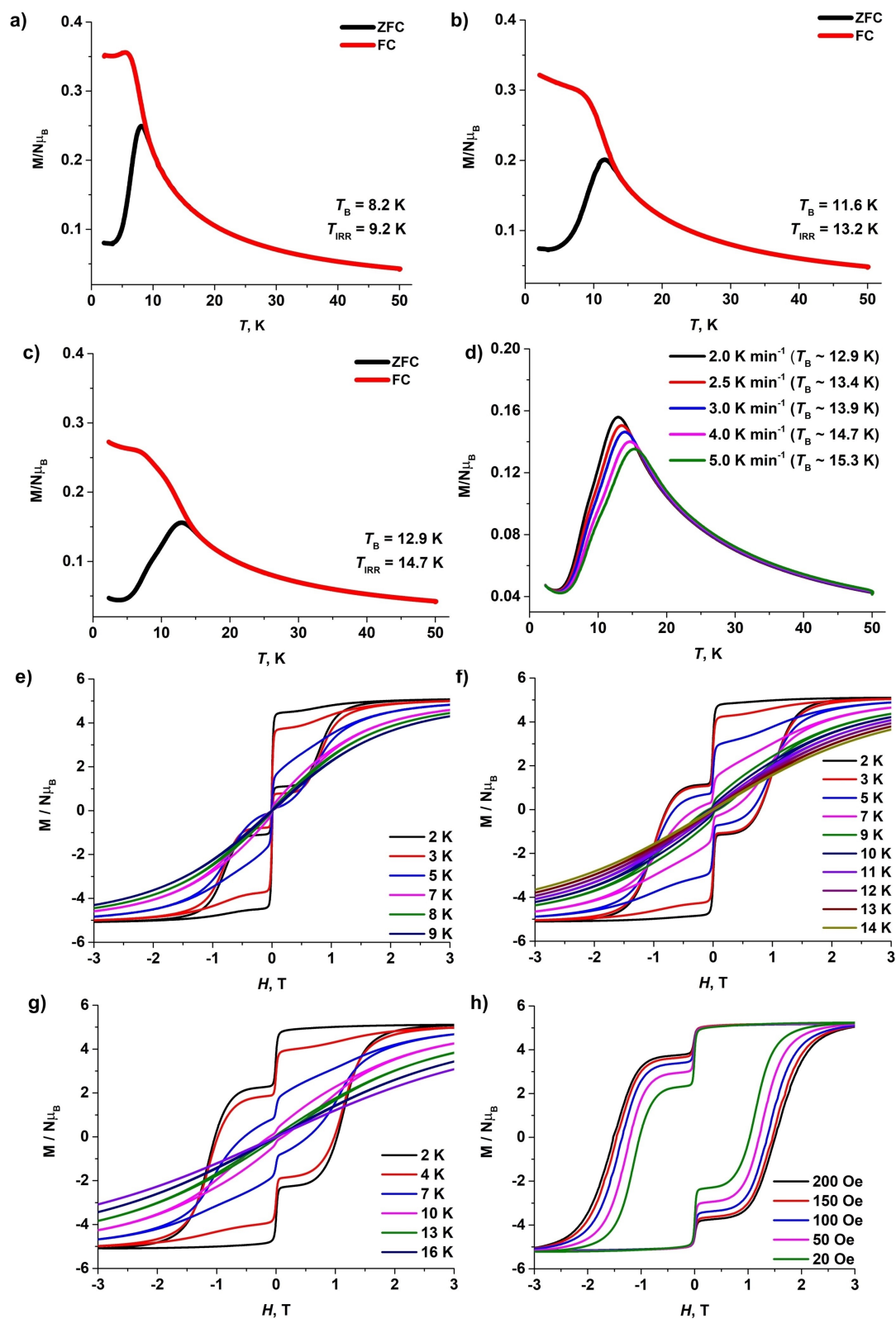


Figure 4. (a–c) Plot of zero field-cooled (black) and field-cooled (red) magnetization vs. temperature for 1–3. (d) Zero field-cooled magnetization vs. temperature for 3 at different temperature sweep rate. (e–g) The field-dependent magnetization data for 1–3 collected at a sweep rate of 20 Oe s⁻¹. (h) Comparative field-dependent magnetization data for 3 at a sweep rate of 20 Oe s⁻¹–200 Oe s⁻¹.

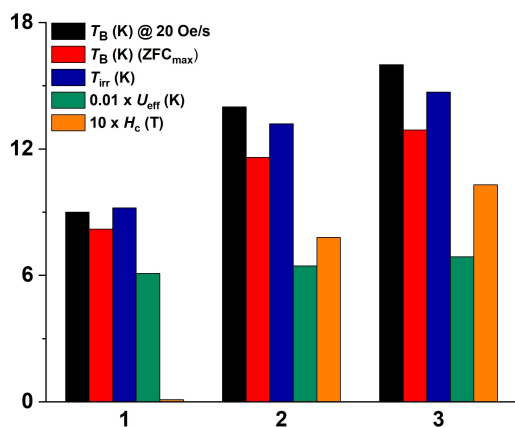


Figure 5. Comparative chart of the magnetic properties of SIMs 1–3.

MOLCAS 8.2 programme package^[15] (see computational details). The chosen *ab initio* methodology was found to provide better guidance to obtain insights and understand the single-ion magnetism shown by lanthanide complexes.^[9d,16] The magnetic anisotropy axis of 1–3 is found to lie along the axial O–Dy–O

bond, perpendicular to the ground state beta electron density^[16a,b,17] to minimize the electrostatic repulsions (Figure 6 and S30–32). The calculations reveal an axial set of g tensors in the ground KD ($g_x = g_y \sim 0.0$; $g_z = 19.857$ (1), 19.878 (2), 19.863 (3), Table S12–14) and first excited KD. This enables negligible QTM/TA-QTM (TA = thermally activated) in the mechanism of magnetization relaxation (Figure 7). Furthermore, the angle of the anisotropy axis between ground and first excited states is found to be $< 6^\circ$. This indicates magnetization relaxation via other higher excited states (Table S12–14). The eight ground KDs generated from the ${}^6H_{15/2}$ state for the three complexes span up to 902.0 (1), 957.7 (2), and 1028.4 K (3). The significant TA-QTM value at the second excited state reinforces the magnetization relaxation ($| -15/2 \rangle \rightarrow | -13/2 \rangle \rightarrow | -1/2 \rangle \rightarrow | +1/2 \rangle \rightarrow | +13/2 \rangle \rightarrow | +15/2 \rangle$, Figure 7). This results in large U_{cal} values of 606.3, 645.7, and 668.9 K for 1, 2, and 3, respectively, consistent with the estimated U_{eff} values (Table S12–14, Figure 7).

To find out the origin of the increasing U_{cal} from 1→2→3, we have estimated the crystal field parameters using the Hamiltonian, $\hat{H}_{CF} = \sum_{k=2,4,6} \sum_{q=-k}^{+k} B_k^q \hat{O}_k^q$ (here B_k^q is the crystal field parameter and \hat{O}_k^q is the Stevens operator respectively). The value of larger axial crystal field (CF) parameter ($k=2, 4, 6$;

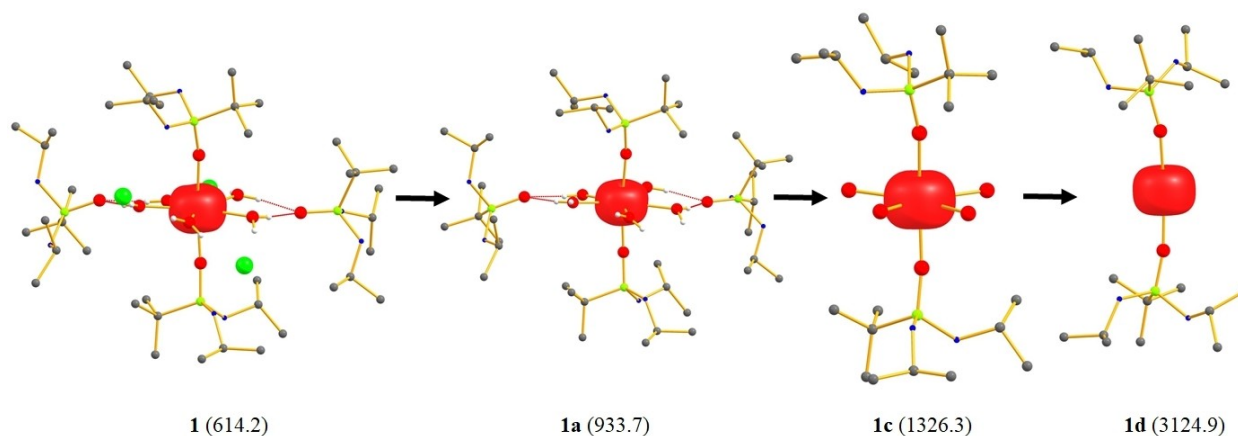


Figure 6. The β -electron density of $m_j = | \pm 15/2 \rangle$ from 1→1a→1b→1c. The number in parenthesis indicates the U_{cal} (K) value from *ab initio* CASSCF/RASSI-SO/SINGLE_ANISO calculations. Colour code: Cl-green, P-light green, O-red, N-blue, C-grey, H-white. Hydrogens (except equatorial hydrogens to show the hydrogen bonding) are omitted for clarity.

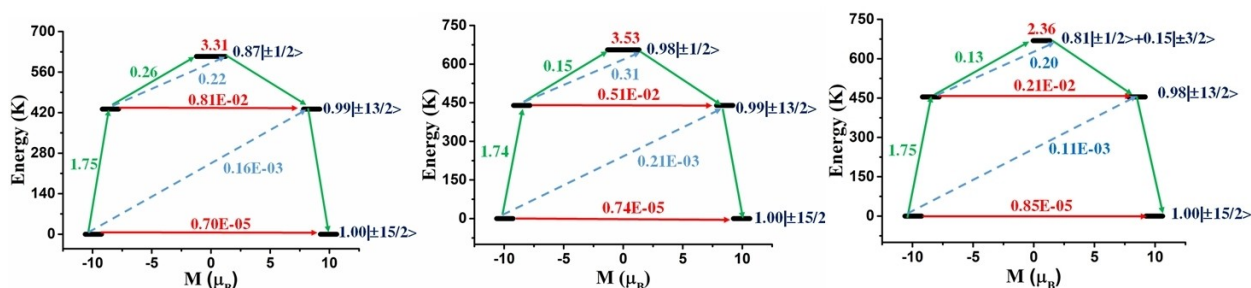


Figure 7. The mechanism of magnetic relaxation of 1 (left), 2 (middle), and 3 (right). The thick black line indicates the Kramer's doublet (KD) as a function of magnetic moment. The red arrow indicates QTM/TA-QTM via ground/excited states. The blue arrow indicates possible Orbach pathway. The green arrow indicates the most probable pathway of magnetic relaxation. The numbers associated with each arrow signifies the mean absolute values of corresponding matrix element of transition magnetic moment. The blue numbers indicate the m_j composition of a KD.

$q=0$) compared to non-axial ($k=2, 4, 6; q \neq 0$) suggests substantial axiality in all the three complexes (Table S15). The higher U_{cal} value of **3** compared to **1** and **2** correlates with the larger axial B_2^0 CF parameter. We have also estimated the $\frac{E_2-E_1}{E_1}$ (E_2 and E_1 is the spin free energy of the first and second excited state, respectively) which is considered as a figure of merit of axiality^[17] in Dy(III) SIM. The larger $\frac{E_2-E_1}{E_1}$ value of **2** and **3** compared to **1** suggests a larger axiality of the former compared to the latter (Table S16). The computed Loprop charges also explain the increasing axiality from **1**→**2**→**3**. The Loprop charges on the equatorial water oxygens vary as $1 < 2 < 3$, but the charge of the surrounding halide counter anions decreases in the order $1 > 2 > 3$ with a more pronounced effect, rationalizing the trend in the $U_{\text{cal}}/U_{\text{eff}}$ values (Table S17). To unravel whether the larger distance between Dy and iodide ions (av. Dy-halide distance is 5.04, 4.80, and 4.56 Å in **3**, **2**, and **1**, respectively) offers a larger U_{cal} value in **3**, we have performed a model calculation on **3-Cl** where the three iodide ions in **3** have been replaced by chloride ions. The calculation on **3-Cl** reveals enhancement of U_{cal} value to 693.4 K (Table S18) compared to **3**, although a significant increase in the Loprop charges of chloride ions is observed (Table S17). This unveils the metal-halide distance rather than the nature of the halide ions controlling the magnetic anisotropy. On the other hand, in our earlier studies, we have established a structural R parameter ($R = \frac{\angle(\text{O}(\text{P})-\text{Dy}-\text{O}(\text{P}))}{1000} + \text{Av.}[(\text{Dy} - \text{Oeq})] - \text{Av.}[\text{Dy} - \text{Oax}])$) to correlate it with the estimated U_{cal} values in *pseudo-D_{5h}* Dy(III) complexes.^[16a] The R value is found to be in the order of $3 > 2 > 1$, which also explains the trend in the U_{cal} values (Table S19).

Further, to analyze the effect of counter anions in magnetic anisotropy, we have removed the halide ions from the secondary coordination sphere of **1**, **2**, and **3** (model **1a**, **2a**, and **3a**, respectively, see Figure 5 and S30-31). Calculations on these models yield enhancement in U_{cal} value to 1032.1, 1115.5, and 1079.5 K for **1a**, **2a**, and **3a**, respectively (Table S20-22). This is due to a reduction in the computed charge for the equatorial oxygen atoms (Table S23-25), compared to the original structure. Quite interestingly, the computed charge of the axial oxygen atoms increases in **1a**, **2a**, and **3a** compared to **1**, **2**, and **3** (Table S23-25). Both these effects lead to the increase in the axial B_2^0 CF parameter (Table S26). For models, the $m_j = |\pm 11/2\rangle$ stabilized as the second excited state, contrary to **1**, **2**, and **3** (Table S20-22) where $m_j = |\pm 1/2\rangle$ was stabilized as second excited state, leading to magnetization relaxation via 3rd excited state (Table S20-22).

To investigate the effect of non-coordinating phosphonamide ligands and halide ions in U_{cal} value, the ligands have been removed from **1**, **2**, and **3**, keeping the halide ions intact (model **1b**, **2b**, and **3b**, respectively, see Figure S32 for beta electron density). The calculations yield a decrease in the U_{cal} value ($U_{\text{cal}}=793.9$ (**1b**), 850.5 (**2b**) and 898.4 K (**3b**)) compared to **1a**, **2a** and **3a** (the magnetization relaxation via second excited state, Table S27-29). In these models, equatorial oxygens were found to possess less charge as their hydrogen bonding solvates/halides were removed, placing their U_{cal} values larger than **1**, **2**, and **3** (Table S23-25). More pronounced changes in the axial/equatorial oxygen charges and the

computed crystal field parameters are observed in models **1a-3a** compared to **1b-3b** (Table S23-25, S30). This suggests that the halide counter anions (equatorial non-bonding interaction with Dy(III)) play a dominant role in magnetic anisotropy compared to the phosphonamide ligands (H-bonding interaction with equatorial water molecules).

In the next step, we have performed calculations on models **1c-3c** where both halides and phosphonamide ligands were removed (see Figure 5 and S30-31). The *ab initio* calculations on these models reveal magnetization relaxation via third excited KD with the increase in the U_{cal} value to 1343.7 (**1c**), 1407.2 (**2c**), 1403.1 K (**3c**) (see Table S31-33) with respect to the original structures and other models constructed. Here the computed values are twice as large as compared to the original structure (2.22 times in **1**, 2.18 times in **2**, 2.09 times in **3**), and this can be rationalized from the computed charges and crystal field parameters (Table S23-25, S34). The U_{cal} value of **2c** is slightly higher compared to **3c** due to the larger O(P)–Dy–O(P) angle found in **2** compared to **3** (Table 1). To obtain the absolute axial limit with these ligands, the equatorial water molecules from **1c-3c** have been removed to build models **1d-3d** (see Figure 5, S30-31 for beta electron density). For these models, calculations reveals magnetization relaxation via 6th excited KD ($m_j: | -15/2\rangle \rightarrow | -13/2\rangle \rightarrow | -11/2\rangle \rightarrow | -9/2\rangle \rightarrow | -7/2\rangle \rightarrow | -5/2\rangle \rightarrow | -3/2\rangle \rightarrow | +3/2\rangle \rightarrow | +5/2\rangle \rightarrow | +7/2\rangle \rightarrow | +9/2\rangle \rightarrow | +11/2\rangle \rightarrow | +13/2\rangle \rightarrow | +15/2\rangle$, Table S35) in **1d** while **2d** and **3d** relaxes via 5th excited KD ($m_j: | -15/2\rangle \rightarrow | -13/2\rangle \rightarrow | -11/2\rangle \rightarrow | -9/2\rangle \rightarrow | -7/2\rangle \rightarrow | -5/2\rangle \rightarrow | +5/2\rangle \rightarrow | +7/2\rangle \rightarrow | +9/2\rangle \rightarrow | +11/2\rangle \rightarrow | +13/2\rangle \rightarrow | +15/2\rangle$, Table S36-37). This leads to the U_{cal} value of 3108.7, 3172.8, and 3188.2 K for **1d**, **2d**, and **3d**, respectively.

The water molecules in **1-3** offer significant equatorial ligation which hinders them from achieving a very large blocking barrier. To decrease the equatorial ligand field in **3**, we have carved out model **3b-acetone** where the five equatorial water molecules in **3b** were replaced by acetone (Figure S33 and Appendix S1 for optimized coordinates). The *ab initio* calculations on **3b-acetone** reveal a decrease in the U_{cal} value to 491.4 K compared to **3** (Table S39). This is due to the loss of planarity in the optimized structure **3b-acetone** (Figure S33). Again, the axial O(P)–Dy–O(P) angle also reduces to 171.48° compared to **3b** (175.16°). Furthermore, we have also performed calculations on **3b-THF** (carved out from **3b** with replacing the equatorial water molecule by THF, Figure S34, Appendix S2) to reduce the equatorial ligation. But the calculations on these models reveal a decrease in the U_{cal} value to 427.1 K due to a decrease of axial O(P)–Dy–O(P) angle (172.22) and loss of equatorial planarity in optimized **3b-THF** compared to **3b** (Table S40).

The unsuccessful attempts to enhance the blocking barrier with model **3b-acetone** and **3b-THF** suggests that the nature of the equatorial donor atom is important compared to its ligand environment in dictating the magnetic anisotropy. Keeping this in mind, we have performed *ab initio* calculation on model **3-H₂S** by replacing the five water molecules of **3** with hydrogen sulfide molecules. The optimized structure of **3-H₂S** leads to a decrease in the axial O(P)–Dy–O(P) angle to 168.64°

and at the same time, the equatorial planarity in **3-H₂S** is also lost compared to **3** (Figure S35 and Appendix S3). The calculations on **3-H₂S** unveil an increase in the U_{cal} value to 1325.9 K compared to **3** with the magnetic relaxation via second excited KD (Table S41). This is due to the reduction of the computed charge of the equatorial sulphur atoms compared to the oxygen atom of the water molecules (Table S42).

Conclusions

In summary, complexes **1–3** present a series of high-performance *pseudo-D_{5h}* Dy(III) SIMs that are isostructural with the same set of ligand systems in the first coordination sphere. Whereas the high anisotropic barrier mostly results from the strong axial phosphoramidate ligands and the higher symmetry around the central Dy(III) ions, the nature of halide ions in the secondary coordination sphere that is hydrogen-bonded to the equatorial coordinated aqua ligand have a profound effect on the relaxation dynamics of the SIMs. The substitution of a larger iodide anion to the smaller strongly hydrogen-bonded chloride anion in the secondary coordination leads to a decrease in the effective energy barrier (U_{eff}) and blocking temperature (T_{b}) in the order **3** > **2** > **1**. Thus, in addition to the first coordination sphere, the secondary coordination sphere can also generate a subsidiary difference in the magnetic properties of SIMs. *Ab initio* calculations aid the understanding of the effects and role of the secondary coordination sphere in modulating the anisotropy of the *D_{5h}* systems. In brief, this study presents anion fine-tuning of a fascinating series of air-stable Dy(III) SIMs and highlights the significance of the careful selection of secondary coordination sphere anions that can have a subtle effect on the overall performance of molecular magnets. Studies, to further fine-tune and understand the effect of other factors, are currently underway in our laboratory.

Experimental Section

Materials, instruments, and methods: All the new compounds reported in this study are stable towards air and moisture and hence all the operations were carried out under normal aerobic conditions. Solvents were distilled before use. The phosphonic diamide ligand, ^tBuPO(NH^tPr)₂ (**L**) was synthesized using a previously reported procedure.^[11] Fourier transform infrared spectra were obtained on a Perkin Elmer Spectrum One FTIR spectrometer as KBr diluted discs. Microanalyses were performed on a Thermo-Finnigan (FLASH EA 1112) microanalyzer. The metal content in the samples was measured by inductively coupled plasma atomic emission spectroscopy (ICP-AES). The samples were digested in nitric acid and diluted with distilled water. The magnetic measurements were carried out on a Quantum Design MPMS-XL SQUID magnetometer equipped with a 7 T magnet in the temperature range 2–300 K using polycrystalline powder samples. The data were corrected for any background diamagnetic contribution using Pascal's constants. Alternating current (ac) susceptibility measurements were carried out in an oscillating ac field of 3.5 Oe and frequencies ranging from 0.1 to 1500 Hz. Hydrated halides salts of Dy(III) and Y(III) were prepared from the corresponding oxides (Alfa Aesar) using suitable mineral acids.

X-ray crystallography: Suitable single crystals of the complexes, obtained from slow evaporation of the solvent from the reaction mixture, were mounted on a Rigaku Saturn 724+ ccd diffractometer for unit cell determination and three-dimensional intensity data collection. Data integration and indexing were carried out using CrystalClear and CrystalStructure.^[18] The structures were solved using direct methods (SIR-97).^[19] Structure refinement and geometrical calculations were carried out using programs in the WinGX^[20] module and Olex2 v1.2.^[21] The final structure refinement was carried out using full least square methods on F^2 using SHELXL-2014.^[22] Details of crystal data and structure refinement are reported in Table S1.

CCDC 1451546 (for **(1)**), 1451547 (for **(2)**), 1812593 (for **(4)**), and 1812594 (for **(5)**) contain the supplementary crystallographic data for this paper. These data are provided free of charge by The Cambridge Crystallographic Data Centre.

Computational details: All the *ab initio* CASSCF/RASSI-SO/SINGLE_ANISO multireference calculation has been performed on the X-ray crystal structures of **1**, **2**, and **3** with MOLCAS 8.2 programme package.^[15] The basis sets for our calculations were taken from the ANO-RCC library implemented in the package.^[23] The following basis set was used throughout the calculations: Dy: [Dy.ANO-RCC.8s7p5d3f2g1h.], I: [I.ANO-RCC.6s5p3d1f.], Br: [Br.ANO-RCC.4s4p2d.], Cl: [Cl.ANO-RCC.4s3p1d.], P: [P.ANO-RCC.4s3p.], S: [S.ANO-RCC.5s4p2d1f.], O: [O.ANO-RCC.4s3p2d1f.], N: [N.ANO-RCC.3s2p.], C: [C.ANO-RCC.3s2p.], H: [H.ANO-RCC.2s.]. The DKH (Douglas-Kroll-Hess) Hamiltonian was used to account for the scalar relativistic effect.^[15] The disk space was reduced by the Cholesky decomposition technique.^[24] The active space for our CASSCF calculation includes nine electrons in seven 4f orbitals, i.e., CAS(9,7). Using this active space, we have computed the energies of 21 sextets which are derived from ⁶H_{15/2} ground state of Dy(III). In the next step, we have mixed 21 sextets to obtain spin-orbit states. In the final step, we have employed SINGLE_ANISO module of MOLCAS to estimate the g tensor, QTM, and blocking barrier. Geometry optimization of models **3-H₂S**, **3-acetone**, and **3-THF** has been carried out with UB3LY functional in Gaussian09 programme package.^[25] The Dy(III) ion has been replaced by Y(III) during optimization. We have used SDD ECP (electron core potential) for Y, and I, Ahlrichs TZVP basis set for S, N and O and SVP basis set C and H.^[26]

General procedure for the synthesis of {[L₂Ln(H₂O)₅][X]₃·L₂·nH₂O}: To a solution of ^tBuPO(NH^tPr)₂ (330 mg, 1.5 mmol) in a solvent mixture of dichloromethane and benzene (4:1 v/v, 30 mL) was added LnX₃·xH₂O (0.25 mmol). The reaction mixture was stirred at 60 °C for 1 h and was cooled down to room temperature. The solution was allowed to stand for some time and was then filtered. The clear filtrate obtained was then kept for crystallization at ambient aerobic conditions. Single crystals were obtained by the slow evaporation of the solvent mixture within a week. The crystals were carefully washed with toluene. A few mL of methanol was necessary for the better dissolution of chloride and bromide salts of Dy(III) and Y(III).

{[L₂Dy(H₂O)₅][Cl]₃·L₂} (1**):** Yield: 0.160 g (52%, based on ligand). Anal. Calcd. for C₄₀H₁₁₀Cl₃DyN₈O₉P₄: C, 38.74; H, 8.94; N, 9.04. Found: C, 38.63; H, 8.82; N, 8.74. FTIR (KBr, cm⁻¹): 3260 (br), 2971 (s), 2873 (w), 1646 (w), 1477 (m), 1424 (s), 1399 (w), 1385 (w), 1369 (m), 1313 (w), 1167 (s), 1131 (vs), 1098 (vs), 1051 (vs), 1028 (s), 943 (w), 910 (m), 886 (w), 830 (w), 659 (m), 511 (w).

{[L₂Dy(H₂O)₅][Br]₃·L₂·H₂O} (2**):** Yield: 0.150 g (43%, based on ligand). M.p.: > 275 °C. Anal. Calcd. for C₄₀H₁₁₂Br₃DyN₈O₁₀P₄: C, 34.53; H, 8.11; N, 8.05. Found: C, 34.63; H, 8.42; N, 8.14. FTIR (KBr, cm⁻¹): 3270 (br), 3178 (br), 2971 (s), 2935 (w), 2873 (w), 1643 (w), 1468 (m), 1422 (s),

1385 (w), 1369 (m), 1312 (w), 1168 (s), 1130 (vs), 1097 (vs), 1050 (vs), 1027 (s), 909 (m), 885 (w), 829 (w), 659 (m), 603 (w), 509 (w).

$[\text{L}_2\text{Y}(\text{H}_2\text{O})_5][\text{Cl}]_3\cdot\text{L}_2\cdot\text{CH}_2\text{Cl}_2$ (4): Yield: 0.175 g (56%, based on ligand). Anal. Calcd. for $\text{C}_{41}\text{H}_{112}\text{Cl}_5\text{N}_8\text{O}_9\text{P}_4\text{Y}$: C, 39.35; H, 9.02; N, 8.95. Found: C, 40.1; H, 9.32; N, 9.47. FTIR (KBr, cm^{-1}): 3262 (br), 2971 (s), 2871 (w), 1655 (w), 1467 (m), 1478 (s), 1427 (s), 1398 (w), 1385 (w), 1367 (m), 1320 (w), 1167 (s), 1132 (vs), 1106 (vs), 1055 (s), 1026 (s), 942 (w), 907 (m), 884 (m), 830 (m), 746 (m), 654 (m), 513 (w). ^1H NMR (CD_3CN , 400 MHz): δ 3.46 (m, 8H, $-\text{CH}(\text{CH}_3)_2$), 1.15–1.21 (m, 84H, $-\text{CH}_3$). ^{13}C NMR (CD_3CN , 100 MHz): δ 42.7, 32.6, 31.4, 25.8, 25.1, 25.0, 24.7. ^{31}P NMR (CD_3CN , 162 MHz): δ 37.2 ppm.

$[\text{L}_2\text{Y}(\text{H}_2\text{O})_5][\text{Br}]_3\cdot\text{L}_2\cdot\text{H}_2\text{O}$ (5): Yield: 0.160 g (49%, based on ligand). Anal. Calcd. for $\text{C}_{40}\text{H}_{112}\text{Br}_3\text{N}_8\text{O}_{10}\text{P}_4\text{Y}$: C, 36.46; H, 8.57; N, 8.50. Found: C, 36.21; H, 8.41; N, 8.82. FTIR (KBr, cm^{-1}): 3262 (br), 2968 (s), 2869 (w), 1477 (s), 1464 (s), 1421 (s), 1387 (w), 1365 (m), 1171 (s), 1132 (vs), 1108 (vs), 1051 (m), 1026 (s), 906 (w), 883 (m), 831 (m), 729 (w), 655 (w), 637 (w), 501 (w). ^1H NMR (CD_3CN , 400 MHz): δ 3.43 (br, 8H, $-\text{CH}(\text{CH}_3)_2$), 3.22 (br, 10H, OH_2), 1.20–1.12 (m, 84H, $-\text{CH}_3$). ^{13}C NMR (CD_3CN , 100 MHz): δ 42.5, 32.5, 31.3, 25.4, 24.6. ^{31}P NMR (CD_3CN , 162 MHz): δ 37.5 ppm.

$[\text{L}_2\text{Dy}_{0.10}\text{Y}_{0.90}(\text{H}_2\text{O})_5][\text{Br}]_3\cdot\text{L}_2\cdot\text{H}_2\text{O}$ (2@5): 2@5 was synthesized using a similar method using 1:9 molar ratios of the respective Dy(III) and Y(III) bromide salts. Yield: 0.140 g (42%, based on ligand). Anal. Calcd. for $\text{C}_{40}\text{H}_{112}\text{Br}_3\text{Dy}_{0.10}\text{N}_8\text{O}_{10}\text{P}_4\text{Y}_{0.90}$: C, 36.25; H, 8.52; N, 8.46. Found: C, 36.13; H, 8.64; N, 8.74. FTIR (KBr, cm^{-1}): 3271 (br), 3181 (br), 2972 (s), 2935 (w), 2873 (w), 1646 (w), 1477 (m), 1422 (s), 1400 (w), 1385 (w), 1369 (m), 1312 (w), 1169 (s), 1131 (vs), 1102 (vs), 1050 (s), 1027 (s), 909 (m), 885 (w), 830 (w), 659 (m), 509 (w).

$[\text{L}_2\text{Dy}_{0.10}\text{Y}_{0.90}(\text{H}_2\text{O})_5][\text{I}]_3\cdot\text{L}_2\cdot\text{H}_2\text{O}$ (3@6): 3@6 was synthesized using a similar method using 1:9 molar ratios of the respective Dy(III) and Y(III) iodide salts. Yield: 0.165 g (45%, based on ligand). Anal. Calcd. for $\text{C}_{40}\text{H}_{112}\text{Dy}_{0.10}\text{I}_3\text{N}_8\text{O}_{10}\text{P}_4\text{Y}_{0.90}$: C, 32.77; H, 7.70; N, 7.64. Found: C, 32.56; H, 7.61; N, 7.78. FTIR (KBr, cm^{-1}): 3286 (br), 2969 (vs), 2909 (m), 2872 (w), 1469 (m), 1420 (s), 1399 (w), 1386 (w), 1368 (m), 1311 (w), 1168 (s), 1131 (vs), 1105 (vs), 1049 (s), 1024 (s), 942 (w), 906 (m), 885 (w), 829 (w), 727 (w), 655 (m), 544 (w), 512 (w).

Acknowledgements

This work was supported by SERB and DST Nanomission (SR/NM/NS-1119/2011), New Delhi, and DAE (BRNS), Mumbai. RM thanks BRNS for the award of DAE-SRC Outstanding Investigator Award (2010/21/04-BRNS/2002) and SERB/DST for a J. C. Bose Fellowship (SB/S2/JCB-85/2014 & 2019). SKG thanks UGC and IRCC, IIT Bombay for a research fellowship. SD thanks to UGC for SRF fellowship. SD thanks to CRAY space time computing facility of IIT Bombay. GR would like to thank DST/SERB for funding (CRG/2018/00430; DST/CSA-03/2018-10; SB/SJF/2019-20/12; SPR/2019/001145).

Conflict of Interest

The authors declare no conflict of interest.

Data Availability Statement

The data that support the findings of this study are available in the supplementary material of this article.

Keywords: anisotropy · axiality · blocking temperature · D_{5h} · dysprosium(III) · single-ion magnet

- [1] a) D. Gatteschi, R. Sessoli, J. Villain, *Molecular nanomagnets*, Oxford University Press, Oxford, 2011; b) D. N. Woodruff, R. E. P. Winpenny, R. A. Layfield, *Chem. Rev.* 2013, 113, 5110–5148; c) J. Tang, P. Zhang, *Lanthanide Single Molecule Magnets*, Springer Berlin Heidelberg, 2015; d) S. K. Gupta, R. Murugavel, *Chem. Commun.* 2018, 54, 3685–3696.
- [2] a) M. Mannini, F. Pineider, P. Saintavit, C. Danieli, E. Otero, C. Sciancalepore, A. M. Talarico, M.-A. Arrio, A. Cornia, D. Gatteschi, R. Sessoli, *Nat. Mater.* 2009, 8, 194–197; b) R. Sessoli, *Nature* 2017, 548, 400–401; c) R. Marin, G. Brunet, M. Murugesu, *Angew. Chem. Int. Ed.* 2021, 60, 1728–1746; *Angew. Chem.* 2021, 133, 1752–1772.
- [3] a) M. Urdampilleta, S. Klyatskaya, J. P. Cleuziou, M. Ruben, W. Wernsdorfer, *Nat. Mater.* 2011, 10, 502–506; b) L. Bogani, W. Wernsdorfer, *Nat. Mater.* 2008, 7, 179; c) M. Mannini, F. Pineider, C. Danieli, F. Totti, L. Sorace, P. Saintavit, M. A. Arrio, E. Otero, L. Joly, J. C. Cezar, A. Cornia, R. Sessoli, *Nature* 2010, 468, 417–421; d) D. Aravena, E. Ruiz, *Dalton Trans.* 2020, 49, 9916–9928.
- [4] a) R. Sessoli, D. Gatteschi, A. Caneschi, M. A. Novak, *Nature* 1993, 365, 141–143; b) A. Caneschi, D. Gatteschi, R. Sessoli, A. L. Barra, L. C. Brunel, M. Guillot, *J. Am. Chem. Soc.* 1991, 113, 5873–5874.
- [5] N. Ishikawa, M. Sugita, T. Ishikawa, S.-Y. Koshihara, Y. Kaizu, *J. Am. Chem. Soc.* 2003, 125, 8694–8695.
- [6] a) J. D. Rinehart, J. R. Long, *Chem. Sci.* 2011, 2, 2078–2085; b) A. J. Brown, D. Pinkowicz, M. R. Saber, K. R. Dunbar, *Angew. Chem. Int. Ed.* 2015, 54, 5864–5868; *Angew. Chem.* 2015, 127, 5962–5966; c) C. A. Gould, K. R. McClain, J. M. Yu, T. J. Groshens, F. Furche, B. G. Harvey, J. R. Long, *J. Am. Chem. Soc.* 2019, 141, 12967–12973; d) Y.-S. Ding, N. F. Chilton, R. E. P. Winpenny, Y.-Z. Zheng, *Angew. Chem. Int. Ed.* 2016, 55, 16071–16074; *Angew. Chem.* 2016, 128, 16305–16308; e) R. J. Blagg, L. Ungur, F. Tuna, J. Speak, P. Comar, D. Collison, W. Wernsdorfer, E. J. L. McInnes, L. F. Chibotaru, R. E. P. Winpenny, *Nat. Chem.* 2013, 5, 673–678; f) S. K. Gupta, T. Rajeshkumar, G. Rajaraman, R. Murugavel, *Chem. Sci.* 2016, 7, 5181–5191; g) L. Sorace, C. Benelli, D. Gatteschi, *Chem. Soc. Rev.* 2011, 40, 3092–3104.
- [7] a) J. D. Rinehart, M. Fang, W. J. Evans, J. R. Long, *Nat. Chem.* 2011, 3, 538–542; b) S. K. Langley, D. P. Wielechowski, B. Moubarak, K. S. Murray, *Chem. Commun.* 2016, 52, 10976–10979; c) S. K. Langley, D. P. Wielechowski, V. Vieru, N. F. Chilton, B. Moubarak, L. F. Chibotaru, K. S. Murray, *Chem. Sci.* 2014, 5, 3246–3256; d) J. D. Rinehart, M. Fang, W. J. Evans, J. R. Long, *J. Am. Chem. Soc.* 2011, 133, 14236–14239; e) S. K. Langley, D. P. Wielechowski, V. Vieru, N. F. Chilton, B. Moubarak, B. F. Abrahams, L. F. Chibotaru, K. S. Murray, *Angew. Chem. Int. Ed.* 2013, 52, 12014–12019; *Angew. Chem.* 2013, 125, 12236–12241.
- [8] a) S. K. Gupta, T. Rajeshkumar, G. Rajaraman, R. Murugavel, *Dalton Trans.* 2018, 47, 357–366; b) F.-S. Guo, B. M. Day, Y.-C. Chen, M.-L. Tong, A. Mansikkamäki, R. A. Layfield, *Angew. Chem. Int. Ed.* 2017, 56, 11445–11449; *Angew. Chem.* 2017, 129, 11603–11607; c) C. A. P. Goodwin, F. Ortu, D. Reta, N. F. Chilton, D. P. Mills, *Nature* 2017, 548, 439–442; d) F.-S. Guo, B. M. Day, Y.-C. Chen, M.-L. Tong, A. Mansikkamäki, R. A. Layfield, *Science* 2018, 362, 1400–1403; e) S. Demir, J. M. Zadrozny, M. Nippe, J. R. Long, *J. Am. Chem. Soc.* 2012, 134, 18546–18549; f) Y.-N. Guo, G.-F. Xu, W. Wernsdorfer, L. Ungur, Y. Guo, J. Tang, H.-J. Zhang, L. F. Chibotaru, A. K. Powell, *J. Am. Chem. Soc.* 2011, 133, 11948–11951.
- [9] a) K.-X. Yu, J. G. C. Kragoskow, Y.-S. Ding, Y.-Q. Zhai, D. Reta, N. F. Chilton, Y.-Z. Zheng, *Chem* 2020, 6, 1777–1793; b) S. K. Gupta, T. Rajeshkumar, G. Rajaraman, R. Murugavel, *Chem. Commun.* 2016, 52, 7168–7171; c) Y.-C. Chen, J.-L. Liu, L. Ungur, J. Liu, Q.-W. Li, L.-F. Wang, Z.-P. Ni, L. F. Chibotaru, X.-M. Chen, M.-L. Tong, *J. Am. Chem. Soc.* 2016, 138, 2829–2837; d) A. B. Canaj, S. Dey, E. R. Martí, C. Wilson, G. Rajaraman, M. Murrie, *Angew. Chem. Int. Ed.* 2019, 58, 14146–14151; *Angew. Chem.* 2019, 131, 14284–14289; e) Z.-H. Li, Y.-Q. Zhai, W.-P. Chen, Y.-S. Ding, Y.-Z. Zheng, *Chem. Eur. J.* 2019, 25, 16219–16224; f) X.-L. Ding, Y.-Q. Zhai, T. Han, W.-P. Chen, Y.-S. Ding, Y.-Z. Zheng, *Chem. Eur. J.* 2021, 27, 2623–2627; g) M. J. Giansiracusa, A. K. Kostopoulos, D. Collison, R. E. P. Winpenny, N. F. Chilton, *Chem. Commun.* 2019, 55, 7025–7028; h) Z.

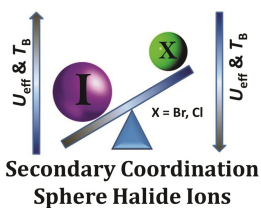
- Zhu, C. Zhao, T. Feng, X. Liu, X. Ying, X.-L. Li, Y.-Q. Zhang, J. Tang, *J. Am. Chem. Soc.* **2021**, *143*, 10077–10082.
- [10] a) V. S. Parmar, F. Ortu, X. Ma, N. F. Chilton, R. Clérac, D. P. Mills, R. E. P. Winpenny, *Chem. Eur. J.* **2020**, *26*, 7774–7778; b) S. Vaidya, S. K. Singh, P. Shukla, K. Ansari, G. Rajaraman, M. Shanmugam, *Chem. Eur. J.* **2017**, *23*, 9546–9559.
- [11] R. Murugavel, R. Pothiraja, *New J. Chem.* **2003**, *27*, 968–974.
- [12] M. Llunell, D. Casanova, J. Cirera, J. Bofill, P. Alemany, S. Alvarez, *SHAPE (version 2.1)*, Barcelona, **2013**.
- [13] a) S. K. Singh, T. Gupta, G. Rajaraman, *Inorg. Chem.* **2014**, *53*, 10835–10845; b) N. F. Chilton, C. A. P. Goodwin, D. P. Mills, R. E. P. Winpenny, *Chem. Commun.* **2015**, *51*, 101–103; c) N. F. Chilton, *Inorg. Chem.* **2015**, *54*, 2097–2099.
- [14] E. Lucaccini, L. Sorace, M. Perfetti, J.-P. Costes, R. Sessoli, *Chem. Commun.* **2014**, *50*, 1648–1651.
- [15] F. Aquilante, J. Autschbach, R. K. Carlson, L. F. Chibotaru, M. G. Delcey, L. De Vico, I. Fdez. Galván, N. Ferré, L. M. Frutos, L. Gagliardi, M. Garavelli, A. Giussani, C. E. Hoyer, G. Li Manni, H. Lischka, D. Ma, P. Å. Malmqvist, T. Müller, A. Nenov, M. Olivucci, T. B. Pedersen, D. Peng, F. Plasser, B. Pritchard, M. Reiher, I. Rivalta, I. Schapiro, J. Segarra-Martí, M. Stenrup, D. G. Truhlar, L. Ungur, A. Valentini, S. Vancouillie, V. Veryazov, V. P. Vysotskiy, O. Weingart, F. Zapata, R. Lindh, *J. Comput. Chem.* **2016**, *37*, 506–541.
- [16] a) M. S. Norre, C. Gao, S. Dey, S. K. Gupta, A. Borah, R. Murugavel, G. Rajaraman, J. Overgaard, *Inorg. Chem.* **2020**, *59*, 717–729; b) P. Kalita, N. Ahmed, A. K. Bar, S. Dey, A. Jana, G. Rajaraman, J.-P. Sutter, V. Chandrasekhar, *Inorg. Chem.* **2020**, *59*, 6603–6612; c) A. B. Canaj, S. Dey, C. Wilson, O. Céspedes, G. Rajaraman, M. Murrie, *Chem. Commun.* **2020**, *56*, 12037–12040; d) A. B. Canaj, S. Dey, O. Céspedes, C. Wilson, G. Rajaraman, M. Murrie, *Chem. Commun.* **2020**, *56*, 1533–1536; e) I. F. Díaz-Ortega, J. M. Herrera, S. Dey, H. Nojiri, G. Rajaraman, E. Colacio, *Inorg. Chem. Front.* **2020**, *7*, 689–699; f) A. Borah, S. Dey, S. K. Gupta, M. G. Walawalkar, G. Rajaraman, R. Murugavel, *Chem. Commun.* **2020**, *56*, 11879–11882; g) S. Dey, G. Rajaraman, *Dalton Trans.* **2020**, *49*, 14781–14785; h) A. B. Canaj, M. K. Singh, C. Wilson, G. Rajaraman, M. Murrie, *Chem. Commun.* **2018**, *54*, 8273–8276; i) A. B. Canaj, M. K. Singh, E. Regincós Martí, M. Damjanović, C. Wilson, O. Céspedes, W. Wernsdorfer, G. Rajaraman, M. Murrie, *Chem. Commun.* **2019**, *55*, 5950–5953.
- [17] D. Aravena, E. Ruiz, *Inorg. Chem.* **2013**, *52*, 13770–13778.
- [18] CrystalClear, Version-SM Expert 2.0 r4, **2009** and CrystalStructure, Version 4.0, Rigaku, **2010**, Rigaku Americas and Rigaku, The Woodlands, Texas, USA and Rigaku Corporation, Tokyo, Japan.
- [19] A. Altomare, M. C. Burla, M. Camalli, G. L. Cascarano, C. Giacovazzo, A. Guagliardi, A. G. Moliterni, G. Polidori, R. Spagna, *J. Appl. Crystallogr.* **1999**, *32*, 115–119.
- [20] L. Farrugia, *J. Appl. Crystallogr.* **2012**, *45*, 849–854.
- [21] O. V. Dolomanov, L. J. Bourhis, R. J. Gildea, J. A. K. Howard, H. Puschmann, *J. Appl. Crystallogr.* **2009**, *42*, 339–341.
- [22] G. Sheldrick, *Acta Crystallogr. Sect. C* **2015**, *71*, 3–8.
- [23] B. O. Roos, R. Lindh, P.-Å. Malmqvist, V. Veryazov, P.-O. Widmark, A. C. Borin, *J. Phys. Chem. A* **2008**, *112*, 11431–11435.
- [24] V. Veryazov, P.-O. Widmark, L. Serrano-Andrés, R. Lindh, B. O. Roos, *Int. J. Quantum Chem.* **2004**, *100*, 626–635.
- [25] a) A. D. Becke, *J. Chem. Phys.* **1993**, *98*, 5648–5652; b) M. J. Frisch, G. W. Trucks, H. B. Schlegel, G. E. Scuseria, M. A. Robb, J. R. Cheeseman, G. Scalmani, V. Barone, B. Mennucci, G. A. Petersson, H. Nakatsuji, M. Caricato, X. Li, H. P. Hratchian, A. F. Izmaylov, J. Bloino, G. Zheng, J. L. Sonnenberg, M. Hada, M. Ehara, K. Toyota, R. Fukuda, J. Hasegawa, M. Ishida, T. Nakajima, Y. Honda, O. Kitao, H. Nakai, T. Vreven, J. A. Montgomery Jr., J. E. Peralta, F. Ogliaro, M. J. Bearpark, J. Heyd, E. N. Brothers, K. N. Kudin, V. N. Staroverov, R. Kobayashi, J. Normand, K. Raghavachari, A. P. Rendell, J. C. Burant, S. S. Iyengar, J. Tomasi, M. Cossi, N. Rega, N. J. Millam, M. Klene, J. E. Knox, J. B. Cross, V. Bakken, C. Adamo, J. Jaramillo, R. Gomperts, R. E. Stratmann, O. Yazyev, A. J. Austin, R. Cammi, C. Pomelli, J. W. Ochterski, R. L. Martin, K. Morokuma, V. G. Zakrzewski, G. A. Voth, P. Salvador, J. J. Dannenberg, S. Dapprich, A. D. Daniels, Ö. Farkas, J. B. Foresman, J. V. Ortiz, J. Cioslowski, D. J. Fox, Gaussian, Inc., Wallingford, CT, USA, **2013**.
- [26] a) A. Schäfer, C. Huber, R. Ahlrichs, *J. Chem. Phys.* **1994**, *100*, 5829–5835; b) T. Dunning, P. Hay, pp. in *Modern Theoretical Chemistry*, Vol. 3, Plenum Press, New York **1977**.

Manuscript received: October 4, 2021
Accepted manuscript online: November 17, 2021
Version of record online: ■■■, ■■■■

FULL PAPER

Bigger the better! The change of hydrogen-bonded halide anions in the secondary coordination sphere of a *pseudo-D*_{5h} Dy(III) single-ion magnet shows a subtle alteration in the magnetic properties. The U_{eff} , T_B and coercivity decrease in the order $I > Br > Cl$ through change of anions in the secondary coordination sphere from larger iodide to smaller chloride ions.

Dy(III) Single-Ion Magnets



Dr. S. K. Gupta, S. Dey, Dr. T. Rajeshkumar, Prof. G. Rajaraman, Prof. R. Murugavel**

1 – 12

Deciphering the Role of Anions and Secondary Coordination Sphere in Tuning Anisotropy in Dy(III) Air-Stable D_{5h} SIMs

